



Sulfasalazine combined with anti-IL-1 β mAb induces ferroptosis and immune modulation in oral squamous cell carcinoma

Rui Zhou^{1,2} · Jiaying Zhou^{1,2} · Yuwen Xiong^{1,2} · Kai Su^{1,2} · Changlin Liu³ · Bin Cheng^{1,2} · Tong Wu^{1,2} 

Received: 11 November 2024 / Revised: 30 April 2025 / Accepted: 5 May 2025
© The Author(s) 2025

Abstract

Oral squamous cell carcinoma (OSCC), one of the most prevalent and aggressive forms of head and neck squamous cell carcinoma, has a five-year survival rate of about 50% ~ 60%, emphasizing the urgent need for more effective therapeutic strategies. Solute carrier family 7 member 11 (SLC7A11) is overexpressed in various cancers and represents a potential therapeutic target. Sulfasalazine (SAS), a Food and Drug Administration-approved drug, is a potent inhibitor of SLC7A11. However, SAS can also increase the levels of pro-inflammatory cytokines such as IL-1 β , which may suppress the immune response. Here, we investigate the effect of SAS combined with anti-IL-1 β monoclonal antibody (anti-IL-1 β mAb) as a novel treatment strategy for OSCC. In this study, SLC7A11 was markedly increased in OSCC tissues, and high SLC7A11 expression predicted poor prognosis. SAS treatment was shown to suppress OSCC cell proliferation and trigger ferroptosis, as evidenced by elevated reactive oxygen species, reduced glutathione and enhanced lipid peroxidation. SAS also elevated IL-1 β levels, leading to T cell exhaustion. Combining SAS with anti-IL-1 β mAb reversed T cell exhaustion and amplified the anti-tumor effects in vitro. In the 4-nitroquinoline-1-oxide-induced oral carcinogenesis model, the combination treatment significantly inhibited oral carcinogenesis compared to monotherapy. Our results suggest that combining SAS with anti-IL-1 β mAb enhances the anti-tumor efficacy against OSCC through tumor growth inhibition and immune modulation, offering a promising therapeutic strategy.

Rui Zhou, Yuwen Xiong and Jiaying Zhou contributed equally to this work.

✉ Bin Cheng
chengbin@mail.sysu.edu.cn

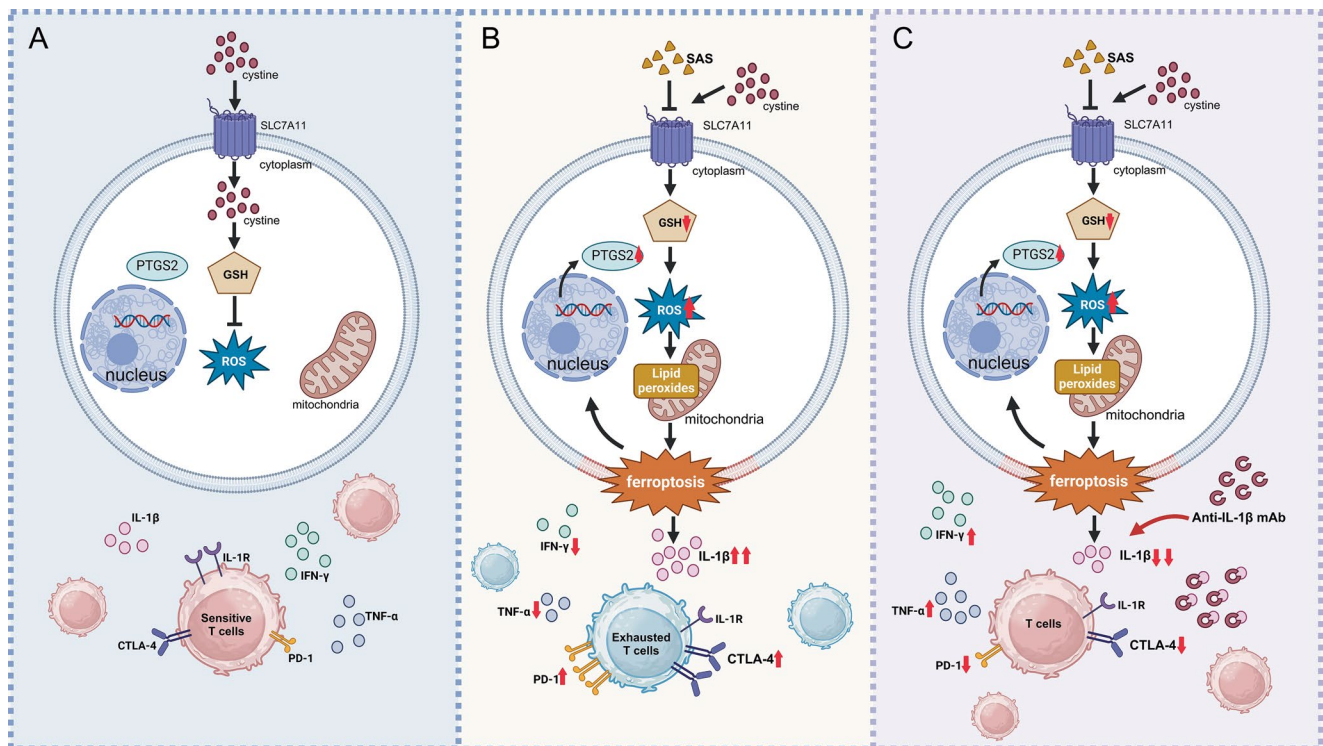
✉ Tong Wu
wutong23@mail.sysu.edu.cn

¹ Hospital of Stomatology, Guanghua School of Stomatology, Sun Yat-sen University, Guangzhou, PR China

² Guangdong Provincial Key Laboratory of Stomatology, Guangzhou 510080, PR China

³ Animal Experiment Center, The First Affiliated Hospital, Sun Yat-sen University, Guangzhou 510080, China

Graphical Abstract



Keywords Solute carrier family 7 member 11 · Interleukin-1 beta · Combined therapy · T cell exhaustion · Oral carcinogenesis

Introduction

Oral cancer is a prevalent global health issue, with approximately 300,000 new cases and 150,000 deaths reported annually [1–3]. Oral squamous cell carcinoma (OSCC), one of the most common types of head and neck squamous cell carcinoma (HNSCC), continues to pose challenges despite advances in surgery, chemotherapy, and radiotherapy [2, 3]. The five-year overall survival rate of OSCC remains approximately 50%–60% [4], emphasizing the urgent need for more effective therapeutic strategies.

Solute carrier family 7 member 11 (SLC7A11, also known as xCT) is a multi-pass transmembrane protein involved in glutathione (GSH) biosynthesis and antioxidant defense. It was highly expressed in many cancers, and high expression of SLC7A11 was associated with poor clinical outcomes [5–7]. Inhibiting SLC7A11 can lead to depleting GSH, making cells more vulnerable to reactive oxygen species (ROS) damage [8]. Considerable interest has been directed toward understanding the role of SLC7A11 in tumor biology and therapeutically targeting SLC7A11 in cancer therapy. Sulfasalazine (SAS), a Food and Drug Administration (FDA)-approved drug commonly used to

treat chronic inflammatory diseases such as rheumatoid arthritis, has been identified as a SLC7A11 inhibitor [9]. Previous studies have demonstrated that SAS inhibited the growth of glioma, melanoma, prostate cancer and non-small-cell lung cancer [10–13], suggesting the therapeutic potential of SAS for cancer treatment. However, the therapeutic effect of SAS in OSCC remains to be fully explored.

SLC7A11 inhibition by SAS induces ferroptosis and oxidative stress, leading to the release of damage-associated molecular patterns (DAMPs), which regulates the immune response and further complicate the immune microenvironment, crucial to OSCC progression and treatment response [14–16]. Emerging evidence suggests a potential link between ferroptosis and the IL-1 pathway, where ferroptosis triggers the release of pro-inflammatory cytokines, including IL-1 β [17–19]. Thus, our study elucidates the role of SAS in modulating IL-1 β and proposes a strategy to optimize the therapeutic efficacy of SAS while mitigating its associated limitations in OSCC.

In this study, we investigate the effects of SAS in OSCC, focusing on its role in ferroptosis and specific immune modulatory effects. The combined approach targeting SLC7A11 and IL-1 β blockade could reverse IL-1 β -dependent

immunosuppression and improve treatment outcomes for OSCC both in vitro and in vivo.

Materials and methods

Cell lines and cell culture

Human normal oral keratinocytes (NOK), human OSCC cell lines SCC1, Cal33, HSC4, human malignant melanoma cell A375 and human breast cancer cell MDA-MB231 were obtained from ATCC (Manassas, VA, USA). NOK, SCC1, Cal33, HSC4, A375 and MDA-MB231 cells were maintained in a Dulbecco's modified Eagle medium (DMEM) high-glucose culture medium (C11995500BT, Gibco, USA) supplemented with 10% (v/v) fetal bovine serum (FS301-02, TransGen Biotech, China), 1% (v/v) penicillin streptomycin (15140122, GIBCO, USA). All cell lines were cultured at 37 °C in a humidified atmosphere containing 5% CO₂.

SLC7A11 expression analysis and survival analysis

The expression level of SLC7A11 gene in a variety of cancer tissues was obtained through the "Gene_DE" module in the TIMER 2.0 (<http://timer.cistrome.org/>), and the statistical significance of differential expression was evaluated using the Wilcoxon test [20]. The RNA-seq data of normal and tumor samples were collected from The Cancer Genome Atlas (TCGA) (<http://cancergenome.nih.gov>). GEPIA (Gene Expression Profiling Interactive Analysis, <http://gepia.cancer-pku.cn/>) is a well-organized website, composed of RNA sequencing data of tumor and normal samples from TCGA and The Genotype-Tissue Expression (GTEx). We employed GEPIA to compare SLC7A11 mRNA expression in normal and HNSCC samples.

Human OSCC samples

Human OSCC samples were obtained from the Hospital of Stomatology, Sun Yat-sen University and informed consent was obtained from each patient. The characteristics of the OSCC patients included in the immunohistochemistry and peripheral blood mononuclear cells analyses were detailed in Supplementary Table 1. The study was approved by the Ethics Committee of the Hospital of Stomatology, Sun Yat-sen University (KQEC-2020-03-17).

Western blot (WB) analysis

SCC1 was cultured in 6-well plates and treated with 800 μ M sulfasalazine (SAS) (HY-14655, MedchemExpress, USA) or/and 50 pM anti-human IL-1 β monoclonal antibody

(anti-IL-1 β mAb) (A2446, Selleck, USA). Protein samples were collected using lysis buffer mixed with a proteinase inhibitor (CW2200S, CWBIO, China). BCA Protein Assay Kit (CW0014S, CWBIO, China) was used to determine protein concentrations. Equal amounts of protein were loaded and separated *via* 10% sodium dodecyl sulfate (SDS) polyacrylamide gel (ET15010LGel, ACE, China) electrophoresis and transferred to polyvinylidene fluoride (PVDF) membranes (ISEQ00010, Merck millipore, USA). The primary antibodies used in this study were as follows: SLC7A11 (1:2000, DF12509, Affinity Biosciences, USA), PTGS2 (1:100000, 66351, Proteintech, USA), IL-1 β (1:1000, ab283818, Abcam, UK) at 4 °C overnight. Bands were detected using Immobilon Western Chemiluminescent ECL Substrate (WBKLSO500, EMD Millipore, USA). The gray value of WB gels was analyzed through Image J software (National Institutes of Health, USA).

Quantitative real-time PCR (q-PCR)

Total RNA of cells was extracted using RNA-Quick Purification Kit (RN001, ESscience, China) and cDNA was synthesized using a Hifair[®] III 1st Strand cDNA Synthesis SuperMix for qPCR (11141ES60, Yeasen, China). The qPCR reactions were performed with a PerfectStart[®] Green qPCR SuperMix (AQ601-01, TransGen Biotech, China) and were run a cycle as preincubation (94 °C for 30s), followed by 40 cycles of amplification (94 °C for 5s, 60 °C for 15s and 72 °C for 10s), a cycle as the melting curve (95 °C for 5s, 65 °C for 60s and 97 °C for 1s) and a final cycle as cooling (40 °C for 10s) in the LightCycler[®] 96 System (Roche, Germany). The following PCR primers were purchased from Tsingke (Guangzhou, China):

GAPDH-F: GGACCTGACCTGCCGTCTAG, GAPDH-R: GTAGCCCAGGATGCCCTTGA. SLC7A11-F: AAG GTGCCACTGTTCATCCC, SLC7A11-R: TGTTCTGGT TATTTTCTCCGACA. PTGS2-F: CTCCTTGGGTGTC AAAGGT, PTGS2-R: AAGTGCTGGGCAAAGAATGC. IL-1 β -F: TGAGCTCGCCAGTGAAATGA, IL-1 β -R: AGA TTCGTAGCTGGATGCCG.

Cell Counting Kit-8 (CCK-8) and 5-Ethynyl-2'-deoxyuridine (EdU) assays

SCC1 cells treated with 800 μ M SAS or/and 50 pM anti-IL-1 β mAb were seeded into plates. Cell proliferation capability was assessed by Cell Counting Kit-8 (CCK-8) assay (T-0012-5000, Telenbiotech, China). EdU assay (C10310-1, RiboBio, China), which focuses on DNA duplication, was performed. Images were captured and analyzed by Image J software.

Reactive oxygen species (ROS) detection

SCC1 was cultured in 6-well plates and treated with reagents as indicated. Cells were then loaded with 2',7'-Dichlorodihydrofluorescein diacetate (DCFH-DA), a fluorescent probe for ROS (CW0014S, Beyotime, China) at a concentration of 10 μ M in all wells. After further culture for 20 min in the dark, the cells were washed twice with 1 mL 1 \times PBS, digested with trypsin to obtain cell pellets and suspended with 500 μ L PBS. LSRFortessa (BD Biosciences, USA) flow cytometer was used to analyze changes in fluorescence. $\lambda_{\text{ex}}=488$ nm, $\lambda_{\text{em}}=530\pm 30$ nm.

Glutathione (GSH) detection

SCC1 was cultured in 6-well plates and treated with reagents as indicated. The supernatant medium was collected and centrifuged at 500 g for 5 min at room temperature to remove floating dead cells and debris. The GSH Quantification kit (BC1175, Solarbio, China) was used to assay GSH level. The measurements were carried out according to the manufacturer's protocols.

Lipid peroxidation assay

Cells were seeded in 6-well plates and treated with drugs for an appropriate time on the next day and then treated with 5 μ M BODIPY 581/591 C11 (D3861, Thermo Fisher Scientific, USA) and incubated at 37 °C for 30 min. The cells were then washed twice with 1 mL 1 \times PBS and the cells were detected by fluorescence spectrophotometer.

Transmission electron microscopy (TEM)

SCC1 cells were seeded in 10 cm culture dishes and incubated overnight. After treated with SAS (800 μ M, 24 h), the cells were trypsinized, rinsed with PBS and fixed with glutaric dialdehyde. Samples were stained with osmium tetroxide and the morphological changes occurring in cells were analyzed by TEM (Hitachi HT7800, Japan). The size of mitochondria was determined by analyzing TEM images with ImageJ software, measuring mitochondrial areas to assess relative size. Damaged mitochondria, identified by shrinkage, increased density, and decreased cristae, were counted manually.

Conditioned medium collection

SCC1 cells were seeded into 6-well plates. Upon treatment with SAS (800 μ M, 24 h), the conditioned medium was collected and centrifuged at 500 g for 5 min at room

temperature to remove floating dead cells and debris and store at -80 °C for use.

Cytometric beads array (CBA)

The variations of cytokines including interleukin-8 (IL-8), interleukin-1 β (IL-1 β), interleukin-6 (IL-6), interleukin-10 (IL-10), tumor necrosis factor- α (TNF- α) and interleukin-12p70 (IL-12p70) in the SAS conditioned medium were detected by Human Inflammatory CBA Kit (551811, BD Biosciences, USA) as the manufacturer's instructions.

Peripheral blood mononuclear cells (PBMCs) isolation, culture and activation

PBMCs were isolated using Ficoll-Paque (TL171440, Telenbiotech, China) density gradient centrifugation from anticoagulant peripheral bloods of enrolled OSCC subjects. Blood cells were centrifuged at 500 g at 20 °C for 30 min with no brake, and PBMCs were collected and washed twice with PBS. PBMCs were plated (5×10^5 per well) in a U-bottom 96-well plate and cultured in RPMI 1640 containing 10% fetal bovine serum and 1 \times penicillin/streptomycin at 37 °C. Cells were treated as follows: (1) control, (2) 40% SAS conditioned medium (prepared by mixing SAS treated supernatant with fresh medium at 2:3 ratio), (3) 30 pg/mL recombinant human IL-1 β (CG93, Novoprotein), (4) 40% SAS conditioned medium + 50 pM anti-human IL-1 β mAb. All groups were stimulated with anti-CD3/CD28 antibodies (final concentration: 1 μ g/mL; Biolegend, 317326/302934) for 48 h.

PBMCs flow cytometry

For intracellular staining of PBMCs, cells were re-stimulated with 50 ng/mL phorbol 12-myristate 13-acetate (PMA) and 100 ng/mL ionomycin (inh-ion, InvivoGen, France) for 4 h in the presence of 1 \times Brefeldin A (BFA; 423303, Biolegend, USA). Cells were blocked with Human TruStain FcX (Fc Receptor Blocking Solution; 422301, BioLegend, USA) on ice for 10 min. Cells were then centrifuged at 500 g for 5 min at 4 °C and washed once with FACS buffer (1 \times PBS with 3% FBS). Cells were incubated for 30 min in the dark at 4 °C with pre-conjugated fluorescence-labeled antibodies including anti-CD4-Alexa Fluor 700 (317426, BioLegend, USA) and anti-CD8-FITC (980908, BioLegend, USA). The cells were then washed once with FACS buffer. Following the washing step, cells were fixed with Fixation Buffer (420801, BioLegend, USA) for 30 min in the dark at 4 °C and then washed twice with Intracellular Staining Permeabilization Wash Buffer (421002, BioLegend, USA) and stained with anti-IFN- γ -BV421 (506538, BioLegend,

USA), anti-PD-1- PE (621608, BioLegend, USA), anti-CTLA-4-APC (369611, BioLegend, USA), and anti-TNF- α -PE (502909, BioLegend, USA) for 30 min at 4 °C in the dark. Cells were then washed twice with Permeabilization Wash Buffer and fixed with 1% PFA. Cells were measured on a LSRFortessa (BD Biosciences, USA) using application settings and at least 20,000 events were collected. Data were then analyzed with FlowJo software (Version 10.0, USA).

Calcein/Propidium Iodide (PI) cell viability assay

SCC1 cells were seeded into 6-well plates and subsequently treated with 800 μ M SAS or/and 50 pM anti-IL-1 β mAb. Jurkat T cells were added to each well at a target-to-effector cell ratio of 1:10 and incubated for 24 h. Cells were then loaded with Calcein Acetoxymethyl Ester (Calcein AM) and PI, a Cell Viability/Cytotoxicity Assay Kit (C 2015 S, Beyotime, China). After further culture for 30 min in the dark, the cells were digested with trypsin to obtain cell pellets and suspended with 500 μ L PBS. LSRFortessa (BD Biosciences, USA) flow cytometer was used to analyze changes in fluorescence. Ex/Em (Calcein AM)=494/517nm, Ex/Em (PI)=535/617nm.

4-nitroquinoline-1-oxide (4NQO)-induced rat oral carcinogenesis model

The 4NQO-induced rat oral carcinogenesis model was established following the procedure in a previous study [21]. Sprague-Dawley (SD) rats (male, 4 weeks) were fed daily with 20 ppm 4NQO solution in their drinking water from week 0 to week 16. After the 16-week carcinogen treatment, the drinking water was switched to distilled water. The rats were divided into 4 groups (6 rats per group) and intratumorally treated from the week 16 as follows: (1) control (150 μ L saline); (2) SAS (150 μ L, 30 mg/kg); (3) anti-rat IL-1 β monoclonal antibody (BE0246, biox-cell, USA) (150 μ L, 100 μ g/kg); (4) SAS (150 μ L, 30 mg/kg)+anti-rat IL-1 β monoclonal antibody (150 μ L, 100 μ g/kg). The rats received intratumoral injections every 3 days for 4 weeks. At the end of week 20, the rats were sacrificed by intraperitoneal injection of pentobarbital sodium and the tongues were dissected, and a longitudinal mid-lingual incision was made. Half of the specimens were fixed in 4% PFA fix solution, embedded in paraffin and cut into 4 mm sections for hematoxylin and eosin (H&E) staining to confirm the pathological diagnosis. The other half of the specimens were stored at -80 °C.

All of the animal procedures were conducted in accordance with the Guidelines for the Care and Use of Laboratory Animals and were approved by the the Ethics Committee of Hospital of Stomatology, SYSU (KQEC-2020-014).

Histopathologic assessment of rat tongue samples


In this study, we followed a procedure that was similar to that in a previous study [21]. The histopathological changes were classified on a 9-point scale to score changes ranging from normal-looking epithelia (a score of 0), to severe invasive carcinoma (a score of 8). The H&E scores were assessed in a blinded fashion by the expert pathologist as follows: 0=normal; 1=hyperplasia; 2=mild dysplasia; 3=moderate dysplasia; 4=severe dysplasia; 5=carcinoma in situ; 6=mild invasion carcinoma, malignant cells deep to basal cell layer, no invasion into 1/3 of the striated muscle; 7=moderate invasion into muscle, no more than 2/3 of the muscle; 8=severe invasion more than 2/3 to the full depth of striated muscle. The results were expressed as the mean score of the histopathological changes for each experimental group.

Immunohistochemistry (IHC)

Immunohistochemical staining was performed according to the manufacturer's instructions. Briefly, the sections of 4NQO-rat tongues were incubated with primary antibodies against SLC7A11 (1:100, DF12509, Affinity Biosciences), PTGS2 (1:200, 66351, Proteintech, USA), IL-1 β (1:500, ab283818, Abcam, USA), Ki67 (1:200, GB151499, Servicebio, China) at 4 °C overnight. Slides were stained using 3,3-diaminobenzidine (DAB; GK600710, Genetech, China) and counterstained using hematoxylin. Pathological sections were scanned and analyzed using an Apreio AT2 digital whole slide scanner (Leica, Wetzlar, Germany). The positive cells were confirmed under 400 \times magnification, and three randomly selected independent microscopic fields were evaluated for each sample to ensure that the data were representative and homogeneous.

Statistical analysis

All the data were analyzed with GraphPad Prism 8 (GraphPad Software, USA). Results were representative of at least three independent experiments and presented as mean \pm the standard error of the mean (SEM). Data normalization was performed relative to the control group. For each experiment, the mean value of the control group was calculated as baseline, and the control and experimental groups were expressed as fold change relative to this baseline. Normality was assessed *via* the Shapiro-Wilk test. For comparisons between two groups, two-tailed unpaired Student's *t*-test (parametric) or Mann-Whitney U test (nonparametric) was applied. One-way ANOVA was used for multiple group comparisons, and Kruskal-Wallis test with Dunn's correction was selected for nonparametric data. All *p*-values

 Springer

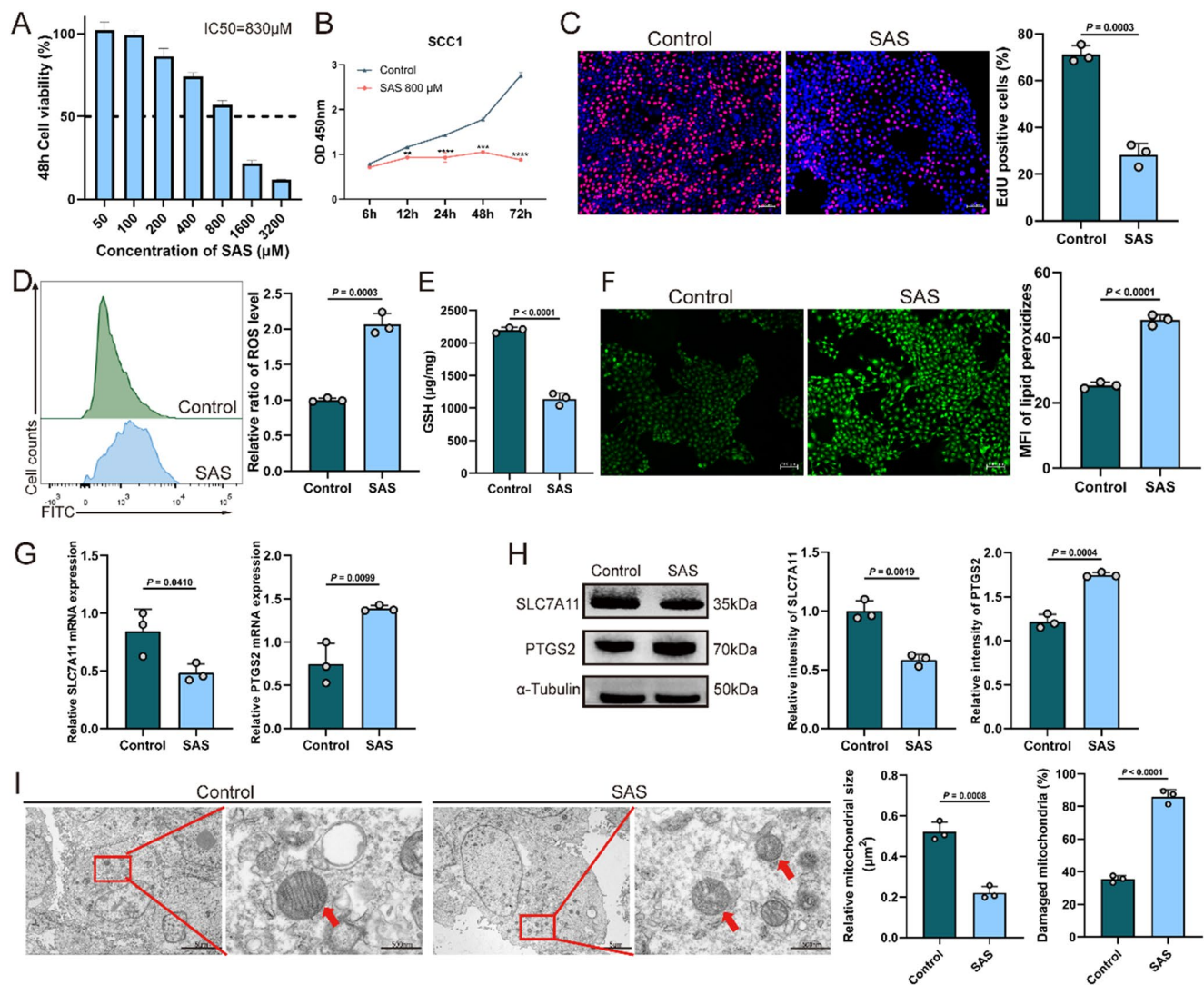


Fig. 2 SAS suppresses OSCC cells proliferation via inducing ferroptosis in vitro. **(A)** Dose-response for SCC1 after exposure to indicated concentrations of SAS for 48 h. IC₅₀ concentrations were listed and error bars indicated SEM for quadruplicate measurements. **(B)** Cell viability of SCC1 after 800 μ M SAS treatment by CCK-8. The differences were considered statistically significant if (*) $P<0.05$, (**) $P<0.01$, (***) $P<0.001$, (****) $P<0.0001$. **(C)** Cell proliferation of SCC1 after 800 μ M SAS treatment for 24 h quantified by EdU assay. Scale bar = 100 μ m. **(D)** Intracellular ROS levels of SCC1 after 800 μ M SAS treatment for 24 h measured by DCFH-DA staining via flow cytometry. **(E)** Intracellular GSH levels of SCC1 after 800 μ M SAS

treatment for 24 h measured by GSH Quantification Kit. **(F)** Lipid peroxidation of SCC1 after 800 μ M SAS treatment for 24 h detected by BODIPY 581/591 C11. Scale bar = 100 μ m. **(G)** Q-PCR experiment of SLC7A11 and PTGS2 expressions in SCC1 after 800 μ M SAS inducing for 24 h. **(H)** Quantitative analysis of WB for SLC7A11 and PTGS2 expressions in SCC1 after 800 μ M SAS inducing for 24 h. **(I)** TEM images of SCC1 cells after 800 μ M SAS treatment for 24 h with analyzed relative mitochondrial size and percentage of damaged mitochondria. Scale bars: 5 μ m and 500 nm. Values are presented as mean \pm SEM. In B-I, unpaired Student's t-test

cells. SAS was found to markedly induce the accumulation of lipid peroxidation products (Fig. 2F). The mRNA and protein levels of the ferroptosis marker PTGS2 were upregulated in SAS-treated cells, and SLC7A11 levels were downregulated (Fig. 2G and H). We also observed the same effect in the OSCC cell lines Cal33 and HSC4 (Supplementary

Fig. 2). TEM of SAS-treated SCC1 cells revealed shrunken mitochondria, increased density and disrupted mitochondrial cristae, indicative of ferroptosis initiation (Fig. 2I).

Taken together, these in vitro results indicate that SAS suppresses OSCC cell proliferation and induces ferroptosis.

SAS-induced accumulation of IL-1 β correlates with T cell exhaustion

The supernatant from SAS-treated SCC1 cells (SAS conditioned medium, SAS CM) was collected for IL-1 β measurement and was subsequently used to treat T cells isolated from PBMCs of enrolled OSCC subjects (Fig. 3A). The levels of IL-8, IL-1 β , IL-6, IL-10, TNF- α and IL-12p70 in the SAS CM were analyzed to assess whether SAS increased pro-inflammatory cytokine secretion and altered the immune microenvironment. The analysis revealed that IL-1 β and IL-10 levels in SAS CM were significantly elevated compared to the control, and TNF- α and IL-12p70 levels were reduced, while IL-8 and IL-6 levels showed no significant changes (Fig. 3B). Additionally, q-PCR and WB analyses demonstrated that SAS treatment increased IL-1 β production in SCC1 cells (Fig. 3C and D), which was further confirmed by elevated IL-1 β levels in SAS CM via ELISA (Fig. 3E).

The impact of SAS CM on T cells was further assessed. Results demonstrated an increase in immune checkpoints, including programmed death 1 (PD-1) and cytotoxic T-lymphocyte antigen 4 (CTLA-4), accompanied by the decrease in TNF- α and interferon- γ (IFN- γ) levels compared to the control (Fig. 3F). These results suggest that SAS CM exerts inhibitory effects on T cells. To confirm whether IL-1 β was responsible for these effects, recombinant IL-1 β was utilized, which replicated the effects observed with SAS CM, confirming that IL-1 β is a key factor driving these inhibitory effects (Fig. 3G).

To further elucidate the role of IL-1 β in OSCC, bioinformatics analysis revealed that IL-1 β expression was significantly elevated in OSCC tissues compared to adjacent tissues in the TCGA dataset (Fig. 3H). This elevation in IL-1 β was associated with a reduction of CD8+ T cells in OSCC patients (Fig. 3I). Additionally, high IL-1 β expression levels were significantly related to poor survival outcomes (Log rank $P=0.03$) (Fig. 3J).

Collectively, these results demonstrate that SAS-induced IL-1 β accumulation is associated with T cell exhaustion in the microenvironment.

Combination of SAS and anti-IL-1 β mAb enhances ferroptosis and inhibits OSCC cell growth

According to the findings above, the inhibition of SLC7A11 by SAS induced ferroptosis and was accompanied with elevated levels of IL-1 β . To counteract the effect of IL-1 β , anti-IL-1 β mAb, a human monoclonal antibody targeting IL-1 β , was introduced. The potential anticancer effects of combining SAS with anti-IL-1 β mAb were investigated, revealing a significant reduction in OSCC cell viability in

Fig. 3 SAS-induced accumulation of IL-1 β correlates with T cell exhaustion. (A) Schematic view of SAS CM and T cells isolated from PBMCs. (B) The levels of IL-8, IL-1 β , IL-6, IL-10, TNF- α and IL-12p70 in the SAS CM analyzed by CBA. (C) Q-PCR experiment of IL-1 β expression in SCC1 after SAS (800 μ M) inducing for 24 h. (D) Quantitative analysis of WB for IL-1 β expression in SCC1 after SAS (800 μ M) inducing for 24 h. (E) The level of IL-1 β in the SAS CM measured by ELISA. (F) Flow cytometric analysis detecting the levels of PD-1, CTLA-4, TNF- α and IFN- γ of 40% SAS CM treating CD8+ T cells. (G) Flow cytometric analysis detecting the levels of PD-1, CTLA-4, TNF- α and IFN- γ of CD8+ T cells treated by 30 pg/mL IL-1 β for 24 h. (H) The expression of IL-1 β in adjacent tissues and OSCC tissues from the TCGA database. (I) The correlation between CD8+ T cell infiltration and IL-1 β expression for OSCC patients in the TCGA database. (J) Kaplan-Meier survival analysis of SLC7A11 expression for OSCC patients in the TCGA database. Values are presented as mean \pm SEM. In B, unpaired Student's t-test or Mann-Whitney U test; C, D, E, F, G and H, unpaired Student's t-test; J, Log-rank test

the combination group compared to either treatment alone, which was also validated in A375 human malignant melanoma cells and MDA-MB231 human breast cancer cells (Fig. 4A and Supplementary Table 2).

To further assess the effects of this combined therapy in the tumor microenvironment (TME), SCC1, A375 and MDA-MB231 cells were cocultured with T cells respectively (Fig. 4B). The combination of SAS and anti-IL-1 β mAb decreased the live cells in all three cell lines compared to SAS treatment alone (Fig. 4C).

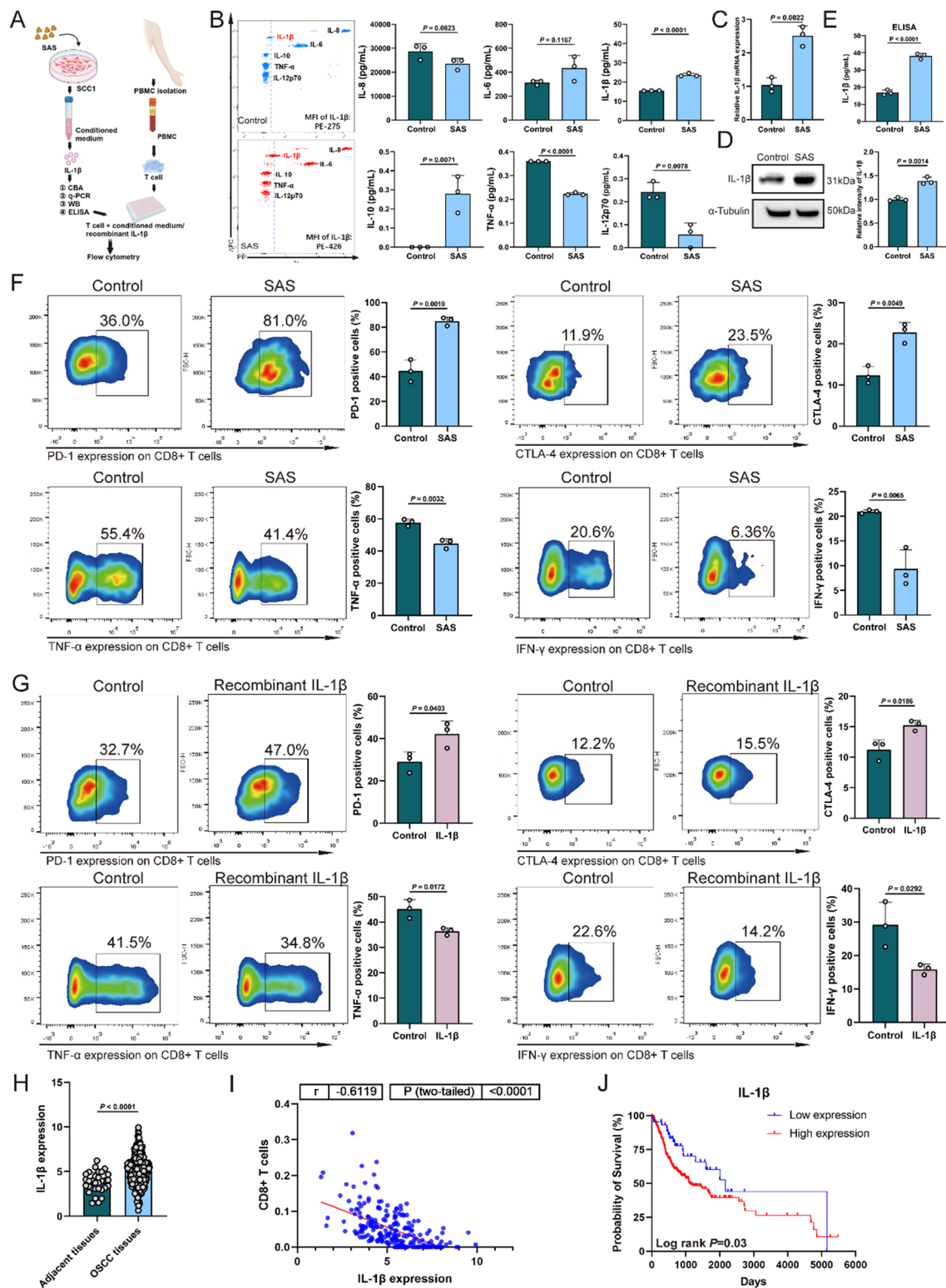
We further investigated whether IL-1 β blockade influenced ferroptosis in SAS-treated SCC1 cells. The combination of SAS and anti-IL-1 β mAb suppressed SCC1 proliferation more effectively than either treatment alone (Fig. 4D). Additionally, the combination treatment resulted in the highest levels of ROS (Fig. 4E) and the lowest levels of GSH (Fig. 4F), along with increased lipid peroxidation (Fig. 4G). Furthermore, the combination treatment significantly reduced both mRNA and protein levels of SLC7A11, while markedly increasing those of PTGS2 (Fig. 4H and I). And the same effects were observed in Cal33 and HSC4 cells (Supplementary Fig. 3).

In conclusion, these results suggest that the combination of SAS and anti-IL-1 β mAb enhances ferroptosis and inhibits OSCC cell growth.

Anti-IL-1 β mAb enhances SAS treatment by reducing IL-1 β level and T cell exhaustion

Reductions in both mRNA and protein levels of IL-1 β were observed in the anti-IL-1 β mAb group and the combination group, confirming the inhibitory effect of anti-IL-1 β mAb on IL-1 β level (Fig. 5A and B). ELISA results further confirmed a decreased concentration of IL-1 β in the combination group compared to the SAS group (Fig. 5C).

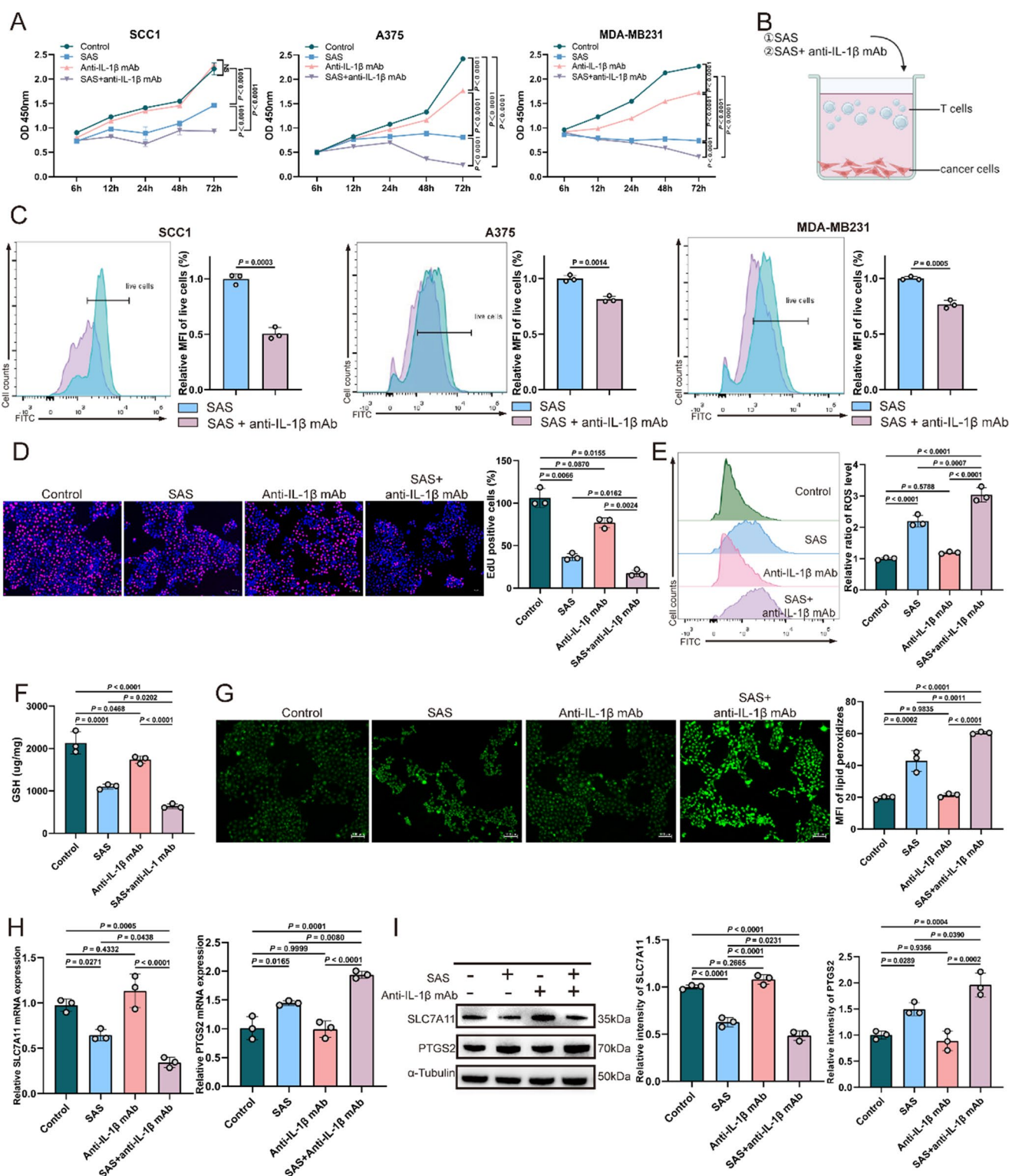
To assess the impact of anti-IL-1 β mAb on T cells and the potential reprogramming of the TME, the conditioned



medium from SCC1 cells treated with SAS (SAS CM), was collected and subsequently applied to T cells with or without the addition of anti-IL-1 β mAb (Fig. 5D). Flow cytometry analysis revealed that SAS CM combined with anti-IL-1 β mAb alleviated T cell exhaustion, as indicated by decreased

levels of PD-1 and CTLA-4 and enhanced production of TNF- α and IFN- γ (Fig. 5E).

In summary, the combined treatment of SAS with anti-IL-1 β mAb not only effectively inhibits IL-1 β production but also alleviates T cell exhaustion.



Combination of SAS and anti-IL-1 β mAb inhibits oral carcinogenesis in 4NQO induced rat model

Since the combination of SAS with anti-IL-1 β mAb significantly inhibited tumor cell growth in vitro, we investigated

its potential to inhibit tumor growth in vivo. A 4NQO-induced oral carcinogenesis rat model was established for this purpose. Following 16 weeks of 4NQO exposure, rats were randomly assigned to four treatment groups: control, SAS, anti-IL-1 β mAb and SAS combined with anti-IL-1 β

Fig. 4 Combination of SAS and anti-IL-1 β mAb enhances ferroptosis and inhibits OSCC cell growth. (A) Cell viability of SCC1, A375 and MDA-MB231 after 800 μ M SAS or/and 50 pM anti-IL-1 β mAb treatment by CCK-8. (B) A diagram of Jurkat T cells and cancer cells co-culture model. (C) Live cells of SCC1, A375 and MDA-MB231 after 800 μ M SAS or/and 50 pM anti-IL-1 β mAb treatment and co-culture with Jurkat T cells for 24 h. (D) EdU assay to quantify cell proliferation of SCC1 after 800 μ M SAS or/and 50 pM anti-IL-1 β mAb treatment for 24 h. Scale bar = 100 μ m. (E) Intracellular ROS levels measured by DCFH-DA staining via flow cytometry. SCC1 cells were incubated with 800 μ M SAS or/and 50 pM anti-IL-1 β mAb treatment for 24 h. (F) Intracellular GSH of SCC1 measured by a GSH Quantification Kit after 800 μ M SAS or/and 50 pM anti-IL-1 β mAb treatment for 24 h. (G) Lipid peroxidation of SCC1 detected by BODIPY 581/591 C11 after 800 μ M SAS or/and 50 pM anti-IL-1 β mAb treatment for 24 h. Scale bar = 100 μ m. (H) Q-PCR experiment of SLC7A11 and PTGS2 expressions in SCC1 after 800 μ M SAS or/and 50 pM anti-IL-1 β mAb inducing for 24 h. (I) Quantitative analysis of WB for SLC7A11 and PTGS2 expressions in SCC1 after 800 μ M SAS or/and 50 pM anti-IL-1 β mAb inducing for 24 h. Values are presented as mean \pm SEM. In A, E, F, G, H and I, one-way ANOVA; C, unpaired Student's t-test; D, Kruskal-Wallis test

mAb (Fig. 6A). Upon completion of the treatments, lesions in the control group developed into cancers accompanied by erosion and ulcers, whereas malignancy was inhibited to varied degrees in the SAS, anti-IL-1 β mAb and combination treatment groups (Fig. 6B and C). Notably, the combination treatment group exhibited the most pronounced inhibitory effect, with a mean H&E score of 3.33, significantly lower than that of the control group (Fig. 6D). The SAS and anti-IL-1 β mAb monotherapy groups also showed significant inhibition, with mean H&E scores of 4, lower than those in the control group (Fig. 6D). Histopathologic assessment of rat tongue samples using H&E staining revealed that in the combination treatment group, only 1 out of 6 cases (16.6%) developed mild invasion carcinoma. In contrast, the control group exhibited more severe outcomes, with 1 out of 6 cases (16.6%) developing carcinoma in situ, 4 out of 6 cases (66.6%) developing moderate invasive carcinoma, and 1 out of 6 cases (16.6%) developing severe invasive carcinoma (Fig. 6E). Monotherapy with either SAS or anti-IL-1 β mAb showed some interruption of the malignant transformation process, but their effectiveness was notably less than in the combination treatment group (Fig. 6D and E).

IHC results indicated that SAS combined with anti-IL-1 β mAb significantly reduced the positive rates of SLC7A11 and IL-1 β , while increasing the positive rate of PTGS2. Additionally, the number of Ki67+ cells significantly decreased in the combination group (Fig. 6F).

Collectively, these findings suggest that the combination of SAS with anti-IL-1 β mAb significantly inhibits carcinogenesis, potentially through the induction of ferroptosis and reverse T cell exhaustion in the 4NQO-induced rat model.

Discussion

OSCC continues to pose a significant global health challenge, with numerous new cases and deaths reported annually [1]. Despite advances in surgical, chemotherapeutic and radiotherapeutic interventions, the overall five-year survival rate for OSCC remains disappointingly about 50% [4], highlighting the need for more effective therapeutic approaches.

To overcome the limitations of current OSCC treatments, the therapeutic potential of targeting SLC7A11, a key component in glutathione synthesis and antioxidant defense, was examined in this study. Significant elevated expression of SLC7A11 in OSCC tissues was demonstrated, consistent with previous findings across various cancers, where high SLC7A11 expression correlated with poor prognosis [10–13]. This was linked to its role in redox homeostasis and ferroptosis vulnerability [22], underscoring the importance of SLC7A11 as the biomarker and therapeutic target.

Following the identification of SLC7A11 as a therapeutic target in OSCC, the potential of SAS, an FDA-approved drug for rheumatoid arthritis, was introduced in this study (Fig. 7). SAS effectively inhibited OSCC cell proliferation by inducing ferroptosis, characterized by increased ROS, lipid peroxidation, and elevated PTGS2 levels, along with decreased GSH and SLC7A11 expression. Additionally, the presence of numerous shrunken mitochondria, a hallmark of ferroptosis initiation, further supported the role of SAS in promoting cancer cell death. These findings aligned with previous studies where SAS inhibited cell proliferation and tumor progression in various cancer models, including non-small cell lung cancer and primary effusion lymphoma [13, 23]. Thus, SAS may represent a promising therapeutic approach for targeting SLC7A11 in OSCC.

Notably, our findings indicated that SAS-induced ferroptosis in OSCC cells led to a significant increase in IL-1 β levels, which contributed to T cell exhaustion and subsequent immunosuppression. IL-1 β is known to regulate ferroptosis in various contexts. Studies suggested that ferroptotic cell death can trigger IL-1 β release, contributing to inflammation and immune modulation [24, 25]. Conversely, IL-1 β signaling may influence ferroptosis susceptibility in cancer cells through the inhibition of nicotinamide nucleotide transhydrogenase acetylation [26]. Thus, there exists a complex interplay between IL-1 β and ferroptosis. Although our data support ferroptosis as a key driver of IL-1 β secretion in SAS-treated OSCC, the causality is partially confounded due to the pleiotropic effects of SAS. Future studies employing IL-1 β knockout models and temporal single-cell analyses are required to distinguish between direct and indirect mechanisms. Additionally, the bidirectional regulation of ferroptosis by IL-1 β highlights a complex feedback loop requiring further exploration.

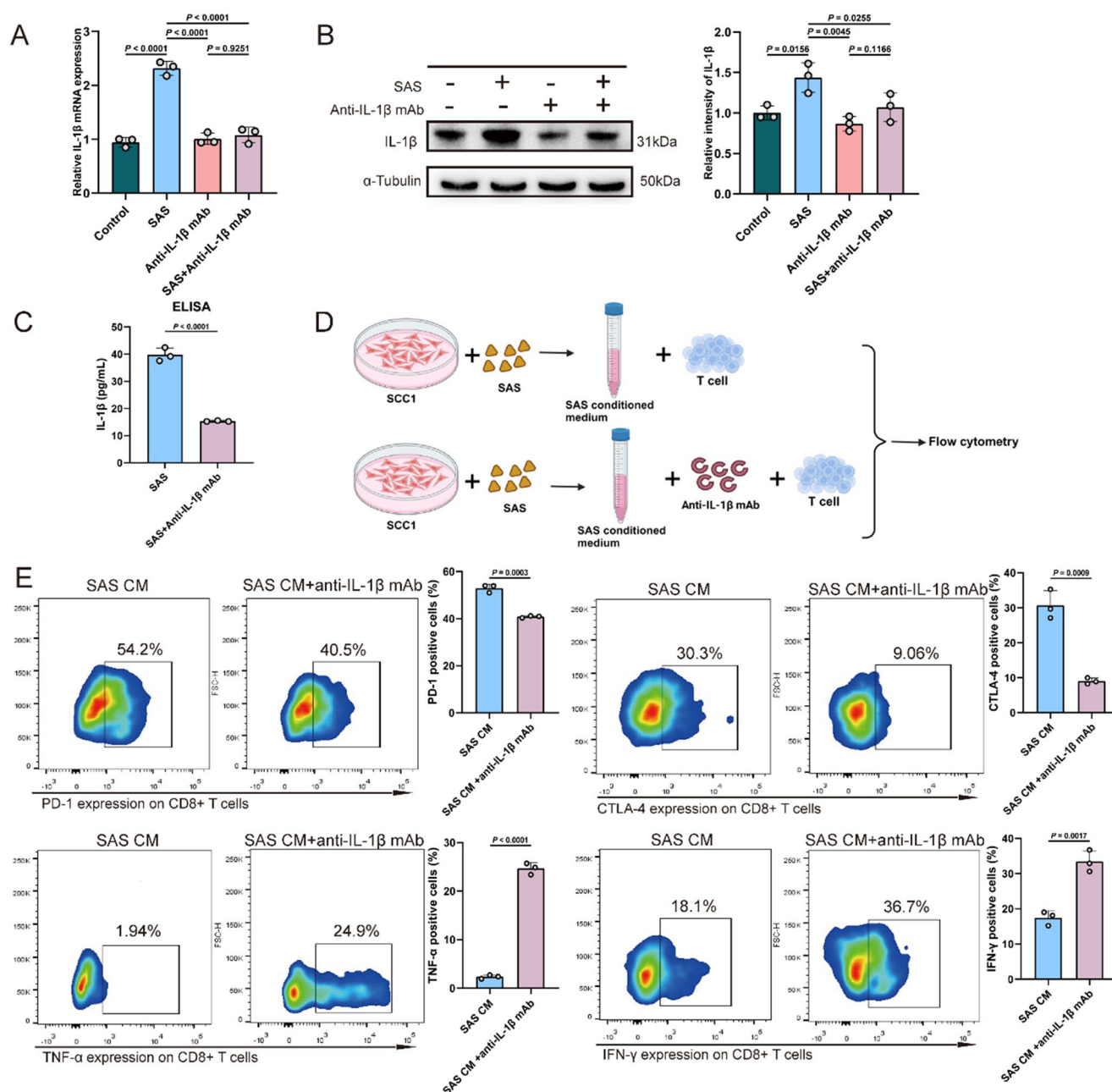


Fig. 5 Anti-IL-1 β mAb enhances SAS treatment by reducing IL-1 β level and T cell exhaustion. **(A)** Q-PCR experiment of IL-1 expression in SCC1 after 800 μ M SAS or/and 50 pM anti-IL-1 β mAb inducing for 24 h. **(B)** Quantitative analysis of WB for IL-1 β expression in SCC1 after 800 μ M SAS or/and 50 pM anti-IL-1 β mAb inducing for 24 h. **(C)** The level of IL-1 β in the SAS and SAS+ anti-IL-1 β mAb

CM measured by ELISA. **(D)** A schematic diagram for flow cytometry. **(E)** Flow cytometric analysis detecting the levels of PD-1, CTLA-4, TNF- α and IFN- γ of 40% SAS CM or with 50 pM anti-IL-1 β mAb treating CD8+ T cells. CD8+ T cells. Values are presented as mean \pm SEM. In A and B, one-way ANOVA; C and D, unpaired Student's t-test

However, it is essential to acknowledge that the TME constitutes a complex ecosystem comprising diverse immune cells, stromal components, and additional cytokines, which were not systematically explored in this study. Although our focus on IL-1 β provides mechanistic clarity, future investigations should encompass these unexplored

factors to achieve a more comprehensive understanding of the interplay between ferroptosis and tumor immunity.

Our data suggest IL-1 β was a mediator of SAS CM-induced T cell exhaustion, while the contribution of other factors present in the conditioned medium requires further elucidation. Future studies employing cytokine profiling or proteomic analysis of SAS CM may identify additional

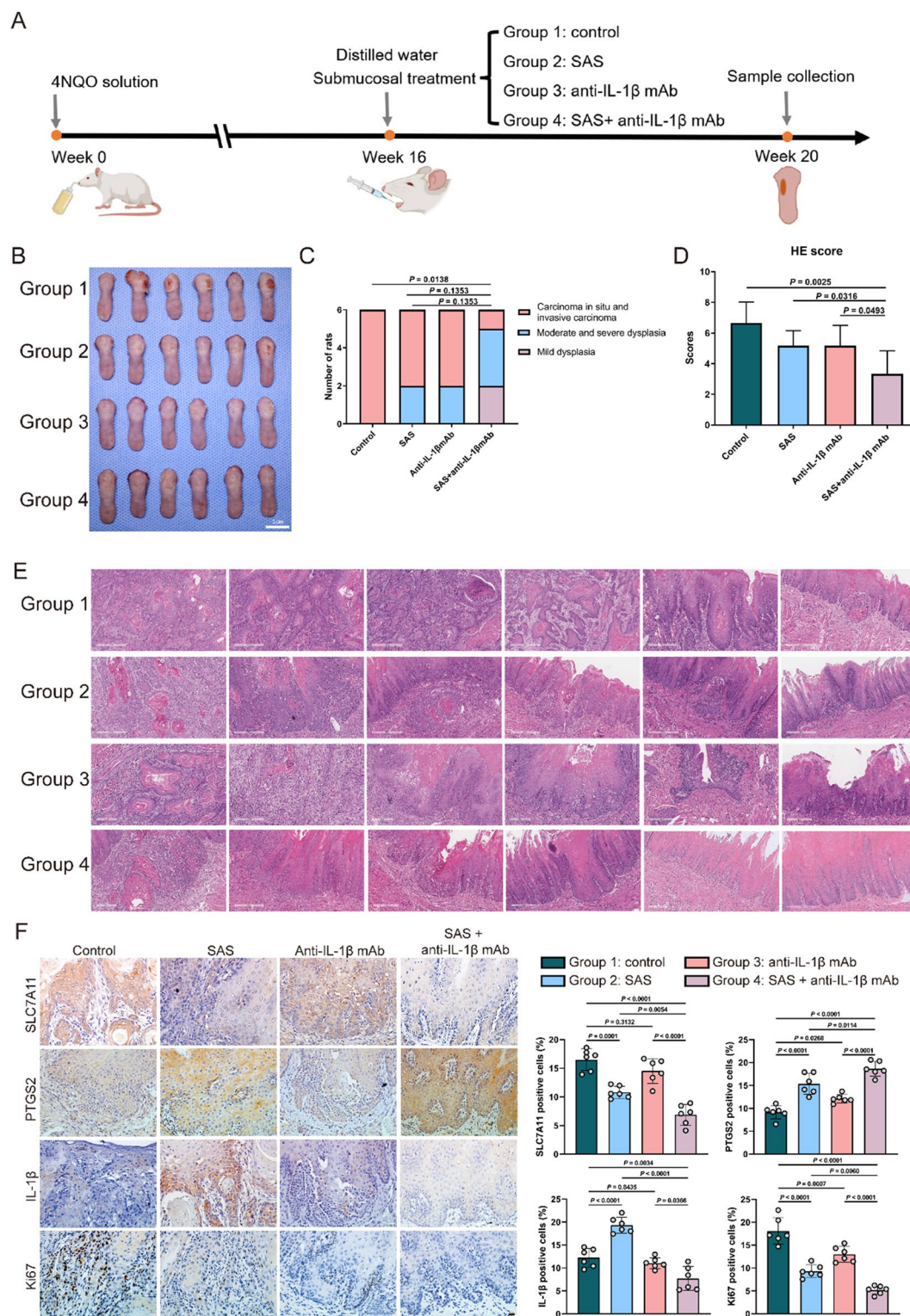


Fig. 6 Combination of SAS and anti-IL-1 β mAb inhibits oral carcinogenesis in 4NQO induced rat model. **(A)** Schematic overview of the 4NQO model experimental design. **(B)** Gross observation of the rat tongues in different groups at the endpoint. Scale bars: 1 cm for gross. **(C)** Quantification of the histological degree of moderate dysplasia, severe dysplasia, and carcinoma in situ and invasive carcinoma in the four groups. **(D)** H&E scores of the histopathological diagnoses in the

four groups. **(E)** Representative H&E images of the rat tongues in different groups at the endpoint. Scale bars: 300 μ m for 10 \times magnification. **(F)** Representative IHC staining of SLC7A11, PTGS2, IL-1 β and Ki67. Data points represent individual rats ($n = 6$ per group). Scale bars: 50 μ m. Values are presented as means \pm SEM. In D and F, one-way ANOVA

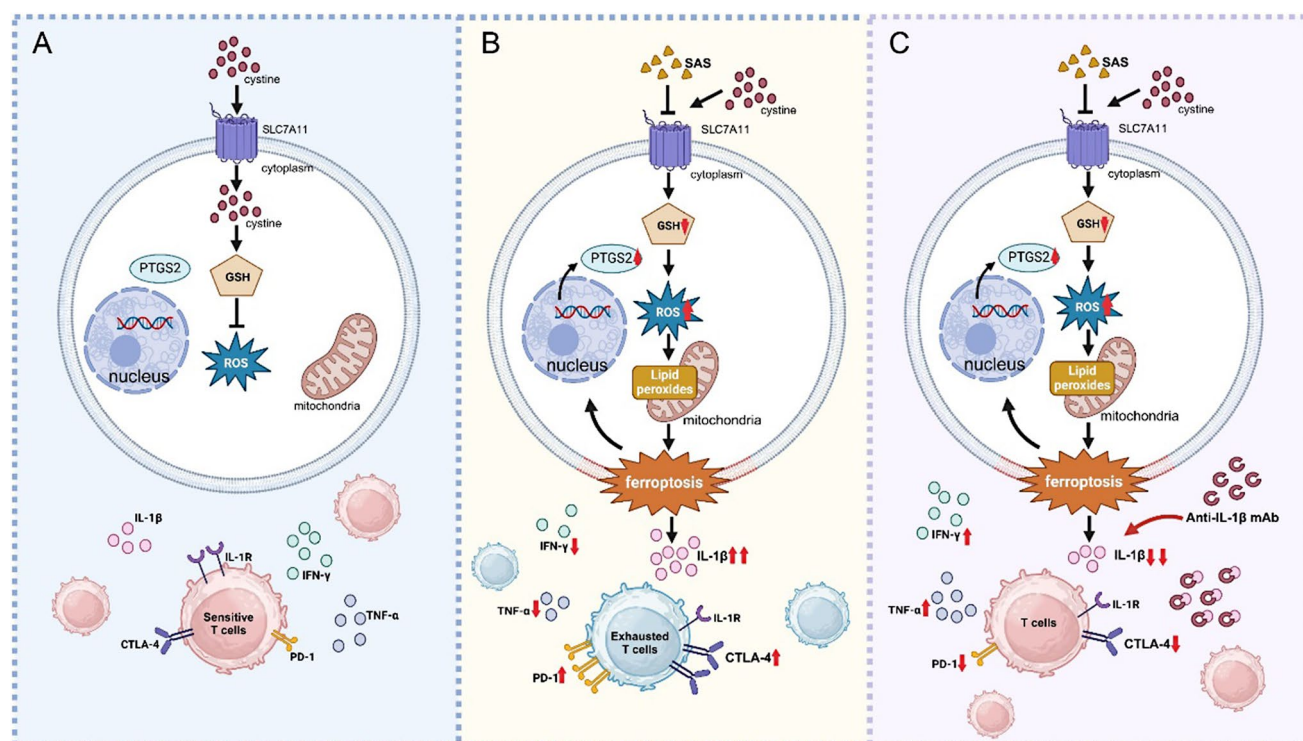


Fig. 7 Schematic model of the combination effect of SAS with anti-IL-1 β mAb. **(A)** SLC7A11 is a crucial transmembrane transporter involved in the extracellular uptake of cystine. Cystine enters cells via SLC7A11, facilitating the synthesis of the potent antioxidant GSH, which mitigates ROS accumulation, prevents lipid peroxidation, and reduces tumor cell death. Within the tumor microenvironment, T cells are present to target and eliminate tumor cells. **(B)** SAS acts as an inhibitor of SLC7A11. SLC7A11 inhibition decreases intracellular GSH levels, and increases ROS production and subsequent lipid per-

oxidation. Concurrently, the expression of PTGS2 rises, inducing ferroptosis in tumor cells. As ferroptosis progresses, a notable increase in IL-1 β secretion is observed within the tumor microenvironment, resulting in T cell exhaustion. **(C)** This T cell dysfunction can be reversed by the addition of anti-IL-1 β mAb. Combined therapy utilizing SAS and anti-IL-1 β mAb effectively targets the vulnerability of iron-dependent cell death, thereby enhancing immune responses and promoting tumor cell destruction

regulators of this process. We also observed changes in other cytokines, such as IL-10, TNF- α , and IL-12p70. Although their absolute levels were low, even small concentrations of cytokines can exert significant biological effects within the TME [27–29]. Further studies are necessary to investigate the mechanistic roles of these cytokine networks and their therapeutic implications.

Our earlier studies identified IL-1 β as a pivotal factor in OSCC progression, where its inhibition disrupted tumor growth by altering the TME [21, 30]. To address the observed immunosuppressive effects, the potential of combining SAS with anti-IL-1 β mAb therapy was investigated as a strategic approach.

The addition of anti-IL-1 β mAb to SAS therapy demonstrated significant potential for enhancing the overall therapeutic effect. This combination notably reduced IL-1 β levels, alleviated T cell exhaustion and enhanced T cell function, as evidenced by decreased PD-1 and CTLA-4 expression and increased TNF- α and IFN- γ production. These findings highlighted the role of IL-1 β in immune suppression within the TME and suggested that blocking IL-1 β

could counter SAS-induced immunosuppression. Anti-IL-1 β mAb, an FDA-approved monoclonal antibody, has demonstrated significant efficacy in various immune-related disorders [31]. In a randomized, double-blind study, anti-IL-1 β mAb was associated with a significant reduction in the occurrence of fatal and non-fatal lung cancers [32]. In our study, the combination of SAS with anti-IL-1 β mAb demonstrated enhanced anti-tumor efficacy compared to either treatment alone. The combination therapy not only enhances the anti-proliferative effects of SAS but also reverses IL-1 β -dependent immunosuppression. This synergy is particularly noteworthy as it addresses both the cancer cells and the immune components of the TME, potentially leading to improved overall treatment outcomes.

The efficacy of the combination therapy was further supported via 4NQO-induced rat model. Our dosing strategy for SAS was based on prior rodent studies demonstrating ferroptosis induction and antitumor efficacy [23, 33]. And the dose of anti-IL-1 β mAb demonstrated potent neutralizing activity, consistent with doses reported in studies of IL-1 β -driven inflammatory models

[24, 34]. The combination of SAS and anti-IL-1 β mAb significantly inhibited tumor development and progression compared to monotherapy, reinforcing the potential of this combined approach for clinical application.

Systemic administration of SAS and anti-IL-1 β mAb may lead to gastrointestinal or immune-related adverse effects. In our study, localized intratumoral delivery mitigates this risk by confining drug exposure to the TME. Intratumoral injection is a viable therapeutic approach for oral cancer [35, 36]. For patients with locally advanced or recurrent OSCC who have surgically inaccessible tumors, intratumoral therapy could serve as a neoadjuvant or palliative treatment option. Furthermore, for the clinical translation of SAS and anti-IL-1 β mAb as a therapeutic strategy, it is essential to validate SLC7A11 and IL-1 β as predictive biomarkers through prospective clinical trials.

The innovative aspect of this study is the combination approach of targeting both SLC7A11 and the immunosuppressive effects of IL-1 β , which provides a more comprehensive therapeutic approach compared to monotherapy, overcoming some limitations of current treatments. Both SAS and anti-IL-1 β mAb are FDA-approved with established safety profiles. Thus, repurposing them for a new indication could lower development costs and accelerate the translation from research to clinical practice [37]. Future studies should evaluate the safety and efficacy of this combination therapy in OSCC patients and explore its potential applicability to other malignancies.

In summary, this study demonstrates that the combination of SAS with anti-IL-1 β mAb effectively induces ferroptosis and modulates IL-1 β -mediated immune responses in OSCC. This innovative strategy suppresses cancer cells and alleviates the IL-1 β -driven immunosuppression, providing preclinical evidence for combining SAS with anti-IL-1 β mAb as a potentially effective and low-cost treatment option for OSCC, with broader applications in oncology.

Supplementary Information The online version contains supplementary material available at <https://doi.org/10.1007/s00018-025-05742-5>.

Acknowledgements This study was supported by the Science and Technology Project of Guangzhou, China (Grant No. 202206080009) and the National Natural Science Foundation of China (Nos. 82370960 and 823B2017). Figure 7 was created with biorender.com.

Author contributions Rui Zhou, Jiaying Zhou and Yuwebn Xiong contributed equally to this work. Conceptualization: Bin Cheng and Tong Wu; methodology, investigation and formal analysis: Rui Zhou, Jiaying Zhou and Yuwen Xiong; resources: Kai Su and Changlin Liu; funding acquisition: Jiaying Zhou, Tong Wu and Bin Cheng; supervision: Bin Cheng; writing - original draft: Rui Zhou and Jiaying Zhou; writing - review and editing: Bin Cheng and Tong Wu. All authors read and approved the final manuscript.

Funding Science and Technology Project of Guangzhou, China (Grant No. 202206080009) and the National Natural Science Foundation of China (Nos. 82370960 and 823B2017).

Data availability Data will be made available on request.

Declarations

Ethical approval All of the animal procedures were conducted in accordance with the Guidelines for the Care and Use of Laboratory Animals and were approved by the the Ethics Committee of Hospital of Stomatology, SYSU (KQEC-2020-014). Research involving human samples was performed in accordance with the Declaration of Helsinki and approved by the Ethics Committee of the Hospital of Stomatology, Sun Yat-sen University (KQEC-2020-03-17).

Conflict of interest The authors declare that they have no known competing financial interests or personal relationships that could have appeared to influence the work reported in this paper.

Open Access This article is licensed under a Creative Commons Attribution-NonCommercial-NoDerivatives 4.0 International License, which permits any non-commercial use, sharing, distribution and reproduction in any medium or format, as long as you give appropriate credit to the original author(s) and the source, provide a link to the Creative Commons licence, and indicate if you modified the licensed material. You do not have permission under this licence to share adapted material derived from this article or parts of it. The images or other third party material in this article are included in the article's Creative Commons licence, unless indicated otherwise in a credit line to the material. If material is not included in the article's Creative Commons licence and your intended use is not permitted by statutory regulation or exceeds the permitted use, you will need to obtain permission directly from the copyright holder. To view a copy of this licence, visit <http://creativecommons.org/licenses/by-nc-nd/4.0/>.

References

1. Bray F, Laversanne M, Sung H et al (2024) Global cancer statistics 2022: GLOBOCAN estimates of incidence and mortality worldwide for 36 cancers in 185 countries. *CA: A Cancer journal for clinicians*. 74(3):229–263. <https://doi.org/10.3322/caac.21834>
2. Aguirre-Urizar JM, Lafuente-Ibañez de Mendoza I, Warnakulasuriya S (2021) Malignant transformation of oral leukoplakia: systematic review and meta-analysis of the last 5 years. *Oral Dis* 27(8):1881–1895. <https://doi.org/10.1111/odi.13810>
3. Sun L, Kang X, Wang C et al (2023) Single-cell and Spatial dissection of precancerous lesions underlying the initiation process of oral squamous cell carcinoma. *Cell Discovery* 9(1). <https://doi.org/10.1038/s41421-023-00532-4>
4. Machiels JP, René Leemans C, Golusinski W et al (2020) Squamous cell carcinoma of the oral cavity, larynx, oropharynx and hypopharynx: EHNS–ESMO–ESTRO clinical practice guidelines for diagnosis, treatment and follow-up. *Ann Oncol* 31(11):1462–1475. <https://doi.org/10.1016/j.annonc.2020.07.011>
5. Yang R, Lai C, Huang L et al (2024) Role of Disulfidptosis in colorectal adenocarcinoma: implications for prognosis and immunity. *Front Immunol* 15:1409149. <https://doi.org/10.3389/fimmu.2024.1409149>
6. Zhang Y, Yao R, Li M et al (2025) CircTTC13 promotes Sorafenib resistance in hepatocellular carcinoma through the Inhibition of

- ferroptosis by targeting the miR-513a-5p/SLC7A11 axis. *Mol Cancer* 24(1):32. <https://doi.org/10.1186/s12943-024-02224-3>
7. Feng L, Zhao K, Sun L et al (2021) SLC7A11 regulated by NRF2 modulates esophageal squamous cell carcinoma radiosensitivity by inhibiting ferroptosis. *J Transl Med* 19(1):367. <https://doi.org/10.1186/s12967-021-03042-7>
 8. Chen X, Kang R, Kroemer G, Tang D (2021) Broadening horizons: the role of ferroptosis in cancer. *Nat Rev Clin Oncol* 18(5):280–296. <https://doi.org/10.1038/s41571-020-00462-0>
 9. Zhou Q, Meng Y, Li D et al (2024) Ferroptosis in cancer: from molecular mechanisms to therapeutic strategies. *Signal Transduct Target Ther* 9(1):55. <https://doi.org/10.1038/s41392-024-01769-5>
 10. Sun S, Guo C, Gao T et al (2022) Hypoxia Enhances Glioma Resistance to Sulfasalazine-Induced Ferroptosis by Upregulating SLC7A11 via PI3K/AKT/HIF-1 α Axis. *Oxid Med Cell Longev*. 2022:7862430. <https://doi.org/10.1155/2022/7862430>
 11. Liu N, Zhang J, Yin M et al (2021) Inhibition of xCT suppresses the efficacy of anti-PD-1/L1 melanoma treatment through Exosomal PD-L1-induced macrophage M2 polarization. *Mol Ther* 29(7):2321–2334. <https://doi.org/10.1016/j.ymthe.2021.03.013>
 12. Zheng Z, Luo G, Shi X et al (2020) The X(c)(-) inhibitor sulfasalazine improves the anti-cancer effect of Pharmacological vitamin C in prostate cancer cells via a glutathione-dependent mechanism. *Cell Oncol (Dordr)* 43(1):95–106. <https://doi.org/10.1007/s13402-019-00474-8>
 13. Ji X, Qian J, Rahman SMJ et al (2018) xCT (SLC7A11)-mediated metabolic reprogramming promotes non-small cell lung cancer progression. *Oncogene* 37(36):5007–5019. <https://doi.org/10.1038/s41388-018-0307-z>
 14. Shi L, Liu Y, Li M, Luo Z (2022) Emerging roles of ferroptosis in the tumor immune landscape: from danger signals to anti-tumor immunity. *FEBS J* 289(13):3655–3665. <https://doi.org/10.1111/febs.16034>
 15. Wen Q, Liu J, Kang R et al (2019) The release and activity of HMGB1 in ferroptosis. *Biochem Biophys Res Commun* 510(2):278–283. <https://doi.org/10.1016/j.bbrc.2019.01.090>
 16. Dai E, Han L, Liu J et al (2020) Autophagy-dependent ferroptosis drives tumor-associated macrophage polarization via release and uptake of oncogenic KRAS protein. *Autophagy* 16(11):2069–2083. <https://doi.org/10.1080/15548627.2020.1714209>
 17. Liu T, Shu J, Liu Y et al (2022) Atorvastatin attenuates ferroptosis-dependent myocardial injury and inflammation following coronary microembolization via the Hif1 α /Ptgs2 pathway. *Front Pharmacol* 13:1057583. <https://doi.org/10.3389/fphar.2022.1057583>
 18. Handa P, Thomas S, Morgan-Stevenson V et al (2019) Iron alters macrophage polarization status and leads to steatohepatitis and fibrogenesis. *J Leukoc Biol* 105(5):1015–1026. <https://doi.org/10.1002/jlb.3a0318-108r>
 19. Wang L, Li X, Chen L et al (2025) Mitochondrial uncoupling Protein-2 ameliorates ischemic stroke by inhibiting Ferroptosis-Induced brain injury and neuroinflammation. *Mol Neurobiol* 62(1):501–517. <https://doi.org/10.1007/s12035-024-04288-0>
 20. Li T, Fu J, Zeng Z et al (2020) TIMER2.0 for analysis of tumor-infiltrating immune cells. *Nucleic Acids Res* 48(W1):W509–w14. <https://doi.org/10.1093/nar/gkaa407>
 21. Wu T, Hong Y, Jia L et al (2016) Modulation of IL-1 β reprogrammes the tumor microenvironment to interrupt oral carcinogenesis. *Sci Rep* 6:20208. <https://doi.org/10.1038/srep20208>
 22. Koppula P, Zhuang L, Gan B (2021) Cystine transporter SLC7A11/xCT in cancer: ferroptosis, nutrient dependency, and cancer therapy. *Protein Cell* 12(8):599–620. <https://doi.org/10.1007/s13238-020-00789-5>
 23. Dai L, Cao Y, Chen Y et al (2014) Targeting xCT, a cystine-glutamate transporter induces apoptosis and tumor regression for KSHV/HIV-associated lymphoma. *J Hematol Oncol* 7:30. <https://doi.org/10.1186/1756-8722-7-30>
 24. Zhan M, Xu H, Yu G et al (2024) Androgen receptor deficiency-induced TUG1 in suppressing ferroptosis to promote benign prostatic hyperplasia through the miR-188-3p/GPX4 signal pathway. *Redox Biol* 75:103298. <https://doi.org/10.1016/j.redox.2024.103298>
 25. Bi X, Wu X, Chen J et al (2024) Characterization of ferroptosis-triggered pyroptotic signaling in heart failure. *Signal Transduct Target Ther* 9(1):257. <https://doi.org/10.1038/s41392-024-01962-6>
 26. Han Y, Zhang YY, Pan YQ et al (2023) IL-1 β -associated NNT acetylation orchestrates iron-sulfur cluster maintenance and cancer immunotherapy resistance. *Mol Cell* 83(11):1887–902e8. <https://doi.org/10.1016/j.molcel.2023.05.011>
 27. Monti M, Ferrari G, Grosso V et al (2023) Impaired activation of plasmacytoid dendritic cells via toll-like receptor 7/9 and STING is mediated by melanoma-derived immunosuppressive cytokines and metabolic drift. *Front Immunol* 14:1227648. <https://doi.org/10.3389/fimmu.2023.1227648>
 28. Zhao S, Jiang J, Jing Y et al (2020) The concentration of tumor necrosis factor- α determines its protective or damaging effect on liver injury by regulating Yap activity. *Cell Death Dis* 11(1):70. <https://doi.org/10.1038/s41419-020-2264-z>
 29. Hewitt SL, Bailey D, Zielinski J et al (2020) Intratumoral IL12 mRNA therapy promotes TH1 transformation of the tumor microenvironment. *Clin Cancer Res* 26(23):6284–6298. <https://doi.org/10.1158/1078-0432.Ccr-20-0472>
 30. Chen X, Lv Q, Hong Y et al (2017) IL-1 β maintains the redox balance by regulating glutaredoxin 1 expression during oral carcinogenesis. *J Oral Pathol Med* 46(5):332–339. <https://doi.org/10.1111/jop.12502>
 31. Lythgoe MP, Prasad V (2022) Repositioning Canakinumab for non-small cell lung cancer-important lessons for drug repurposing in oncology. *Br J Cancer* 127(5):785–787. <https://doi.org/10.1038/s41416-022-01893-5>
 32. Ridker PM, MacFadyen JG, Thuren T et al (2017) Effect of interleukin-1 β Inhibition with Canakinumab on incident lung cancer in patients with atherosclerosis: exploratory results from a randomised, double-blind, placebo-controlled trial. *Lancet* 390(10105):1833–1842. [https://doi.org/10.1016/s0140-6736\(17\)32247-x](https://doi.org/10.1016/s0140-6736(17)32247-x)
 33. Song Y, Jang J, Shin TH et al (2017) Sulfasalazine attenuates evading anticancer response of CD133-positive hepatocellular carcinoma cells. *J Exp Clin Cancer Res* 36(1):38. <https://doi.org/10.1186/s13046-017-0511-7>
 34. Yuan B, Clowers MJ, Velasco WV et al (2022) Targeting IL-1 β as an immunopreventive and therapeutic modality for K-ras-mutant lung cancer. *JCI Insight* 7(11). <https://doi.org/10.1172/jci.insight.157788>
 35. Yin Q, Zhang J, Zhang H et al (2024) Cascade nanoreactor employs Mitochondrial-Directed chemodynamic and delta-ALA-Mediated photodynamic synergy for Deep-Seated oral Cancer therapy. *Adv Health Mater* 13(19):e2304639. <https://doi.org/10.1002/adhm.202304639>
 36. Zhang S, Gong L, Sun Y et al (2025) An ultra-long-acting L-asparaginase synergizes with an immune checkpoint inhibitor in starvation-immunotherapy of metastatic solid tumors. *Biomaterials* 312:122740. <https://doi.org/10.1016/j.biomaterials.2024.122740>
 37. Xia Y, Sun M, Huang H, Jin WL (2024) Drug repurposing for cancer therapy. *Signal Transduct Target Ther* 9(1):92. <https://doi.org/10.1038/s41392-024-01808-1>

Publisher's note Springer Nature remains neutral with regard to jurisdictional claims in published maps and institutional affiliations.